J Electroceram (2006) 16: 167–178
DOI 10.1007/s10832-006-6202-y

In situ X-ray diffraction studies of electroceramics

S. T. Misture

Received: 25 February 2005 / Revised: 21 September 2005 / Accepted: 11 November 2005

Abstract In-situ high temperature powder X-ray diffraction is in the midst of a renaissance enabled by new X-ray optics, detectors, computational methods, and furnace designs. In-situ diffraction, under controlled temperature, atmosphere, pressure, electric and magnetic field, etc. has enabled many studies of materials systems that are not easily studied using the more traditional quenching methods. A brief overview of the current capabilities of high temperature diffraction in the laboratory is presented. Examples center on ionic and electronic conductors and capabilities for controlling temperature and oxygen partial pressure that are so often critical in the study of electroceramics.

Keywords High temperature diffraction · Ionic conduction · Electronic conduction · Fuel cell

Introduction

X-ray powder diffraction is among the most common tools used in the study of materials, with applications ranging from fundamental scientific studies to materials engineering and process optimization. The diffraction methods are well suited for studies over a wide range of length scales, beginning, of course, with atomic-scale crystal structures. Microstructural features in the range of $\sim$ 5 to 1000 nm, including crystallite size and microstrain, are apparent in the diffraction line shape and width. Crystallite texture and macro-scale residual stress analysis, as well as phase quantification, extend the length scale out to the bulk macroscopic level.

S. T. Misture
New York State College of Ceramics at Alfred University
Alfred, New York 14802, USA
misture@alfred.edu

Incorporating non-ambient sample chambers into the diffractometer system provides a means of studying the dynamics of a material or material system response to external variables that include temperature, pressure, gaseous atmosphere, electric field, magnetic field, etc., and combinations thereof. In-situ diffraction methods therefore enable studies of material systems that can not be 'quenched in' and analyzed in an ambient environment, and also provide a means of rapid, accurate, and efficient analysis of systems that are traditionally studied using the quenching method. Several fairly recent book chapters [1–4] and even one text [5] provide comprehensive reviews of in-situ diffraction using laboratory diffractometers as well as synchrotron and neutron sources, with most of the literature focused on mineralogy and geology.

It is clear from the literature that the vast majority of in-situ diffraction studies of inorganic materials has been performed using either neutrons or synchrotron radiation. In the past few years, however, revolutionary improvements in laboratory powder diffraction systems, combined with the need to understand more and more complex materials systems, has led to more widespread use of laboratory systems for in-situ diffraction. An overview of modern in-situ diffraction capabilities is therefore presented, with a focus on laboratory X-ray sources, highlighting applications in the study of electroceramics.

Overview of current capabilities

Four major components comprise the in-situ diffractometer: the diffraction furnace, the optical components used to condition the X-ray beam, the detection system, and the environmental control system that might include gas and vacuum systems, magnetic and electric field sources, etc. Most

current in-situ XRD systems simply incorporate a diffraction furnace in a standard laboratory diffractometer. Several laboratory diffraction furnaces that allow simultaneous control of temperature and atmosphere have been commercially available for at least two decades [4, 5], most of which use a resistively-heated metal strip to control the temperature of the specimen. Using a metal strip to heat and support the specimen offers the advantages of rapid heating and cooling rates, and a variety of metal heaters to reach temperatures in excess of 2000°C in inert atmosphere. The primary disadvantage is temperature uniformity across the specimen, which generally requires careful temperature calibration [5].

In the past few years, several new custom furnaces have been designed and tested [6–9], and several new commercial devices have been marketed. The defining characteristic of the newer designs is a large heated volume, on the order of 100–500 cm^3 which, in principle, affords uniform temperatures regardless of the dimensions of the specimen.

Currently, there exists only one commercial diffraction furnace that allows full 3-D motion of the specimen so that full texture and stress analysis can be performed under controlled temperature and atmosphere. The others facilitate only two-circle diffraction measurements, including powder diffraction, omega-tilt residual stress, and potentially thin film diffraction and reflectivity, etc.

Revolutionary advances in detector technology occurred in 2004 and 2005, which impact all aspects of laboratory diffraction. The traditional XRD instrument uses a point detector that is either step-scanned or continuously scanned over the angular range of interest, with data collection times ranging from perhaps 10 minutes (for a qualitative analysis of one or two peaks) to 20 hours (for data of quality necessary for a structure solution). Faster detectors include a range of 1- and 2-dimensional position-sensitive detectors (PSDs) that simultaneously capture a fixed angular range of scattered X-rays as shown in Fig. 1. The revolutionary new detectors are high dynamic range solid-state detectors in both 1-D and 2-D geometries.

At the time of writing, it is not clear that the 2-D detectors have even been tested for in-situ XRD experiments. However, 1-D PSDs are commonly used for in-situ studies, with active areas of ∼1–5 cm in length, providing simultaneous data collection over an angular range of some 2 to 12°2θ. Curved linear PSD systems can collect a wider range of diffracted intensity, up to approximately 120°2θ.

Typical experiments using a linear PSD of 5 cm length involve scanning the PSD to measure the diffracted signal over the range of interest using a scan rate of 5–20°2θ/min. Therefore, the total time to collect each diffraction pattern is generally 3 to 25 minutes. More rapid experiments can be performed by fixing the PSD at the angle of interest and collecting only the angular range intercepted by the detector (see Fig. 1). In the case of a 5 cm PSD, this might be 12°2θ, which is often sufficient to monitor several diffraction peaks simultaneously. The measurement time per pattern with the PSD fixed is generally 30–300 seconds. For strongly-diffracting samples it is possible to take snapshots as short as 2 seconds per pattern [10], or even at the millisecond scale for cyclic events where the diffracted intensities can be integrated over some large number of cycles [11].

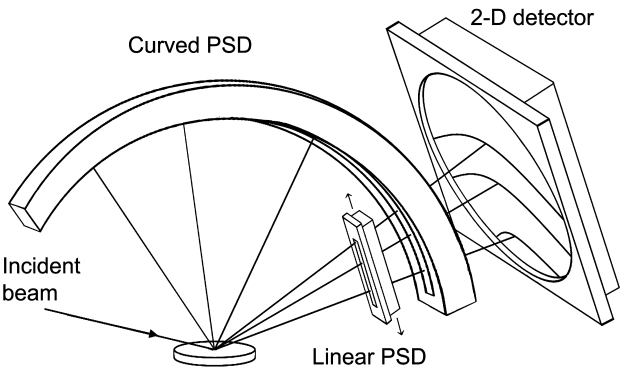

Fig. 1 Schematic of a diffraction system equipped with a linear position-sensitive detector (PSD), a curved PSD, and an area detector

Over the past 5 years, new laboratory X-ray optics have become commercially available that provide a simple and reliable means of reducing many sample-related errors, in particular specimen surface displacement. The optical configuration for laboratory diffraction has historically been the Bragg-Brentano parafocusing geometry. Parafocusing diffractometers are unfortunately exquisitely sensitive to systematic specimen displacement errors, which is a major concern for any studies that require accurate lattice constants [12]. Systematic specimen displacement errors are often amplified by heating or cooling the specimen, and therefore must be carefully considered.

New X-ray optical elements that include graded multilayers, channel-cut crystals, and mono- and poly-capillary lenses, can be used to condition the beam with high efficiency to improve upon the spectral purity of the beam and/or to control the beam divergence. The optical elements that produce "parallel" beams with total beam divergence less than ∼0.04° reduce the sensitivity to specimen displacement, and therefore provide a means of obtaining high accuracy lattice constants even if specimen displacements occur on heating [13–17]. With hardware and software improvements that allow "quick change" of optics and sample holders, it is now feasible to optimize the diffractometer arrangement with minimal effort for the particular measurement.

Most commercial in-situ XRD systems allow some level of atmosphere control. Important considerations for a diffraction furnace are the heating and cooling rates, maximum

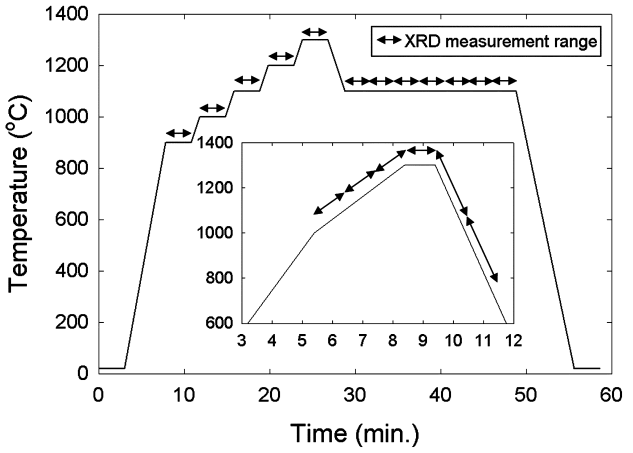

Fig. 2 Typical time-temperature profiles used in in-situ XRD experiments. The main figure shows an isothermal series, while the inset shows a dynamic measurement during which XRD data are measured during heating, cooling, or isothermally

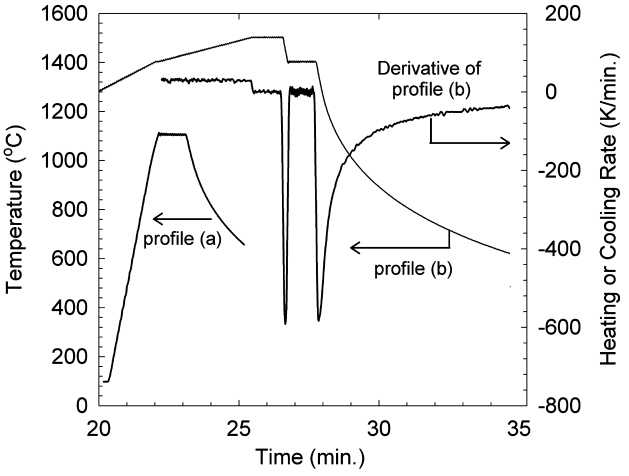

Fig. 4 Measured sample temperatures demonstrating the maximum controlled heating and cooling rates. Profile (a) is the temperature profile at the sample position during a programmed 600°C/min heating and cooling cycle to 1100°C. Profile (b) shows two different heating rates, and again a 600°C/min programmed cooling rate

temperature, and degree of atmosphere control. The maximum heating and cooling rates are important for studies of reaction kinetics, while the atmosphere control capabilities are critical for flexibility. For example, a system that is amenable to high vacuum and atmospheres of pure O_2 to pure H_2 and humidity might be useful in the study of solid oxide fuel cells.

In-situ XRD experiments may be performed under isothermal and non-isothermal conditions, as shown schematically in Fig. 2. Isothermal measurements involve heating or cooling the specimen to some target temperature, then collecting XRD data while the temperature is held constant. The alternative approach is to heat or cool the specimen at a constant rate and collect XRD data during heating or cooling. Naturally, the latter method introduces a temperature change during the measurement, but is applicable for the study of rapid reactions or for developing time-temperature profiles for rapid thermal processing.

Experimental details

Much of data shown in the following sections were collected using one of two different custom in-situ XRD systems developed at Alfred University, shown in Fig. 3. Both systems incorporate mBraun linear PSDs, and one is equipped for standard Bragg-Brentano divergent beam measurements, while the second includes parallel incident and diffracted beam conditioning using graded multilayer optics [7, 9]. Both diffraction furnaces operate to 1600°C under any gaseous atmosphere including hydrogen. The maximum controlled heating and cooling rates are on the order of 600°C/min., as shown in Fig. 4.

The divergent beam system is in vertical geometry, which is convenient for experiments that include reaching peritectic temperatures or fully melting specimens and then tracking recrystallization, simply because the specimen remains

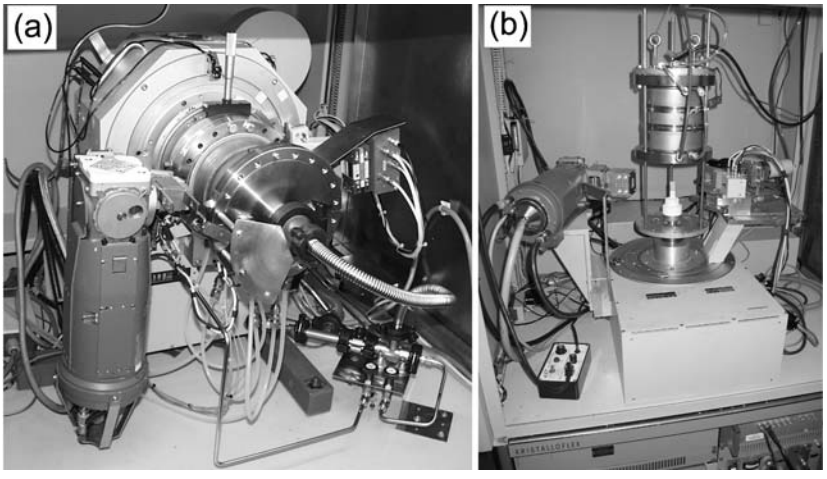

Fig. 3 Photographs of the two custom in-situ XRD systems used in the studies. (a) is the vertical geometry Bragg-Brentano instrument and (b) is the horizontal system that employs multilayer optics for parallel beam operation

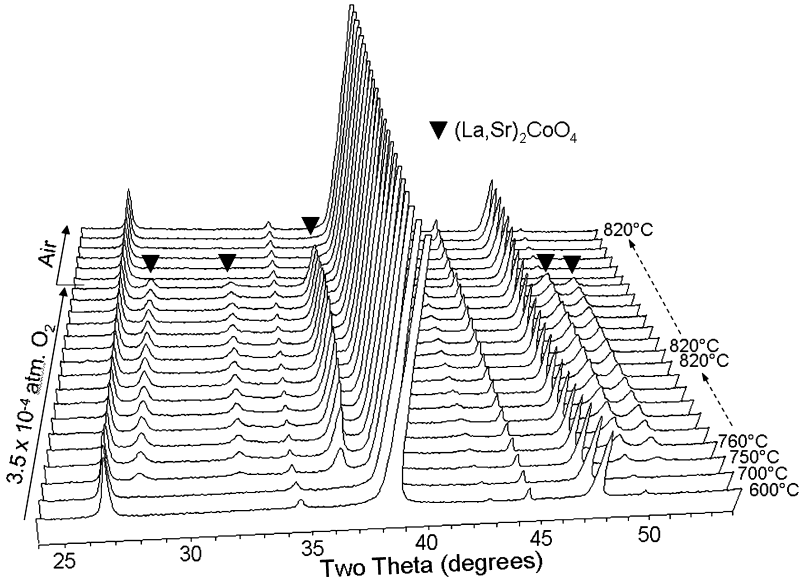

Fig. 5 in-situ XRD patterns that show phase separation of LSC when heated under He/O_2 at $pO_2 = 3.5 \times 10^{-4}$ atm., and then holding isothermally for ~17 hours. A step change to air reverses the phase separation during the isothermal hold

horizontal throughout the experiment. The horizontal system that employs multilayer optics can accommodate samples contained in capillaries, thus providing a "micro-reactor" environment if the sample of interest is sealed within a capillary under reactive gas, for instance. In addition, the horizontal system allows both transmission and reflection measurements and has two permanently-mounted detector systems, the first a PSD and the second a point detector with a diffracted-beam multilayer optic. The latter is well-suited for collecting data for unit cell indexing and structure solutions at high temperature. An additional advantage of the horizontal in-situ XRD system is that the furnace is raised and lowered by a motorized system. Therefore, the furnace can be preheated to a target temperature while above the specimen, and then lowered over the specimen to attain the fastest possible heating rate. Naturally, the ability to preheat the furnace is of great value in studies of reaction kinetics where it is important to have well-defined time resolution and a reliable estimate of the "$t = 0$" experiment starting point.

Applications in electroceramics

The perovskite mixed ionic–electronic conductors such as (La, Sr)$CoO_{3-\delta}$ (LSC) have potential application in a wide range of electrochemical devices, and have recently been revisited because of their complex expansion behavior and questionable phase stability at low oxygen partial pressures [18–22]. The anomalously high "chemical expansion" is attributed to a large population of oxygen vacancies [23, 24] which unfortunately can not be modeled simply as an increase in the B-site cation radius upon reduction [18, 23, 24].

Although quenching specimens from prescribed temperatures and oxygen partial pressures is useful, Chen, et al.[18] point out that uncertainties in interpretation of the data may arise. In-situ diffraction studies of (La, Sr)(Co, Fe)$O_{3-\delta}$ [19, 21, 25] and $LaMnO_3$ [20] have provided accurate phase diagrams and a clear picture of the effects of oxygen content on cell volume and distortion. An example of our ongoing work on LSC is shown in Fig. 5, which is the first clear evidence of phase instability in LSC at low Sr content and low pO_2. Figure 5 shows that heating $La_{0.8}Sr_{0.2}CoO_{3-\delta}$ at $pO_2 = 3.5 \times 10^{-4}$ atm. results in rapid phase separation to form (La, Sr)$CoO_{3-\delta}$, CoO, and $(La, Sr)_2CoO_4$. Reoxidation of the specimen at 820°C using a step change in the oxygen pressure to 0.21 atm. reverses the phase separation.

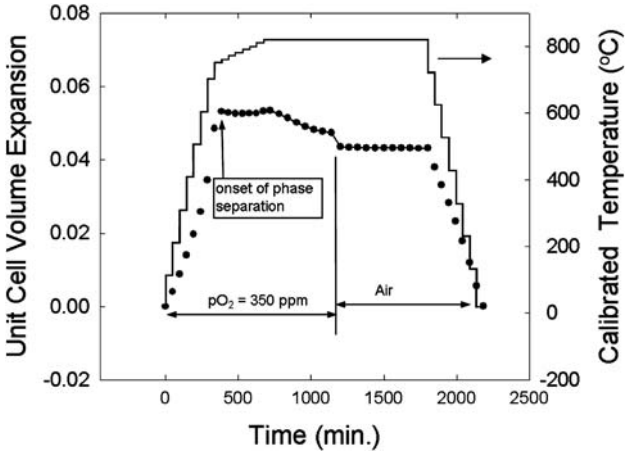

Fig. 6 Unit cell volume thermal expansion extracted from the data in Fig. 5, demonstrating the slow isothermal relaxation of the expansion at $pO_2 = 3.5 \times 10^{-4}$ atm. and the change in chemical expansion on reoxidation

Diffraction data provide, of course, a means of determining the thermal expansion, and provide microstructural information including the size of coherent diffracting domains. Figure 6 shows the thermal expansion of the LSC phase on heating and during an isothermal hold of ~17 hours, extracted from the data shown in Fig. 5. Phase separation occurs on heating, and then the LSC phase slowly equilibrates to smaller expansion values over the course of the 7-hour isothermal hold at 820°C and $pO_2 = 3.5 \times 10^{-4}$ bar. As expected, the pO_2 transient to 0.21 bar during the isothermal hold reduces the chemical expansion, which remains stable over the duration of the experiment, but also reverses the phase separation.

The curious decrease of the LSC cell volume during the initial 7 hours of the isothermal hold, which is far too sluggish to be simply related to anion diffusion, was recently detected by Chen et al. [18] who used dilatometric measurements of bulk samples over long time periods and obtained similar results. Chen et al. suggest that the slow variation in expansion with time may result from phase instabilities

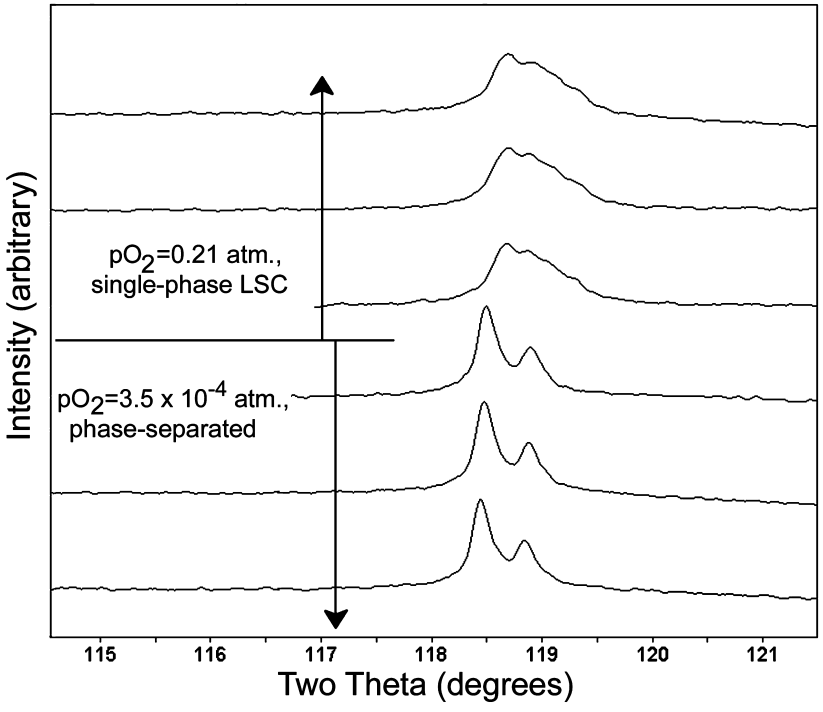

Fig. 7 Broadening of the pseudo-cubic (321) line of LSC on reoxidation resulting from a decrease in the coherent diffracting domain size from 900 to 170 nm

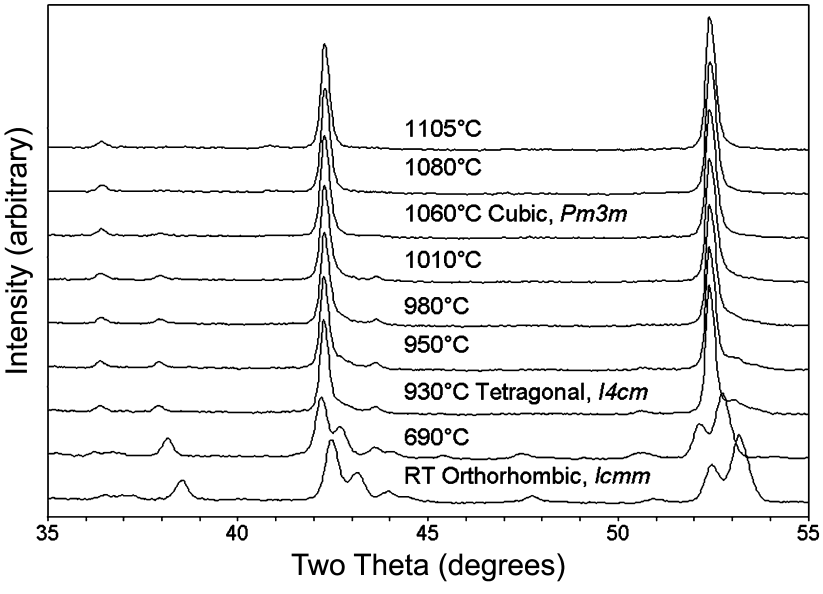

Fig. 8 In-situ XRD data used to track the unit cell symmetry of $Ba_2In_2O_5$ during heating

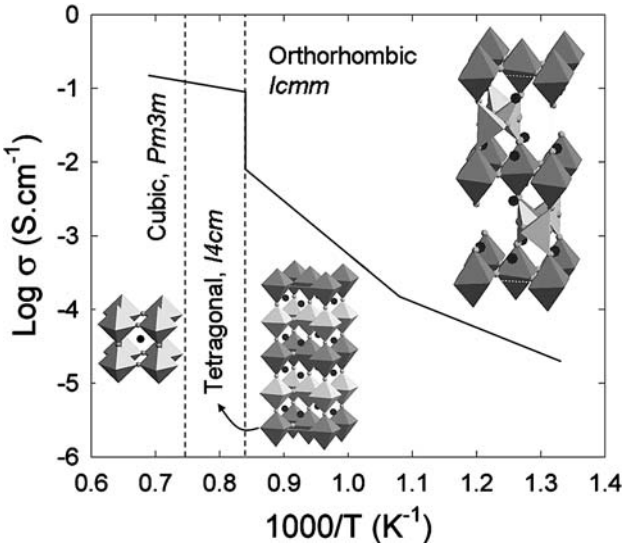

Fig. 9 The final structures of $Ba_2In_2O_5$ determined from both X-ray and neutron diffraction, correlated with the measured ionic conductivity

and/or local interactions such as microdomain formation. Figure 7 shows the effect of the isothermal reoxidation on the diffraction peak width, and clearly shows a significant increase in the diffraction peak width as the phase separation is reversed to form pure $La_{0.8}Sr_{0.2}CoO_{3-\delta}$. Rietveld analysis of the data result in coherent diffracting domain sizes of 900 and 170 nm for the LSC phase under reducing conditions and after reoxidation, respectively. High resolution TEM imaging and electron diffraction have been used to detect regions of Sr/La segregation ranging in size from 8–40 nm [26] and ~100 nm microdomains attributed to vacancy ordering [27]. The X-ray diffraction results are in therefore in reasonable agreement with the TEM data, and additional experiments are in progress to better understand the subtle structural changes that occur over long time periods.

Another example of a materials system that is not amenable to quench studies is the fast ion conductor $Ba_2In_2O_5$ that undergoes an order-disorder transformation at high temperature. Oxide ion conduction in the Brownmillerite structure type has been studied since 1990, when Goodenough et al. [28] reported an order-disorder transformation in $Ba_2In_2O_5$ leading to fast ion conduction above ~925°C. $Ba_2In_2O_5$ and its analogs have since been the subject of many studies linking the structures to the temperature dependence of the conductivity and behavior in the presence of water, CO_2, and under reducing conditions. (see for example [29–33])

Figure 8 shows the in-situ XRD data for $Ba_2In_2O_5$ up to 1105°C, in which the orthorhombic to tetragonal to cubic phase transformations are obvious. Although the XRD method is insensitive to the oxygen sublattice, the in-situ XRD measurements show the phase transformations clearly, and unambiguously provide the time dependence of the phase transformations. Additional neutron powder diffraction experiments at high temperature were undertaken [32] to fully define the oxygen site occupancies, and the resulting crystal structures were linked to the conductivity as shown in Fig. 9. The in-situ diffraction studies clearly demonstrate that fast ion conduction in $Ba_2In_2O_5$ correlates with disordering of the oxygen vacancies in two dimensions, on transforming to

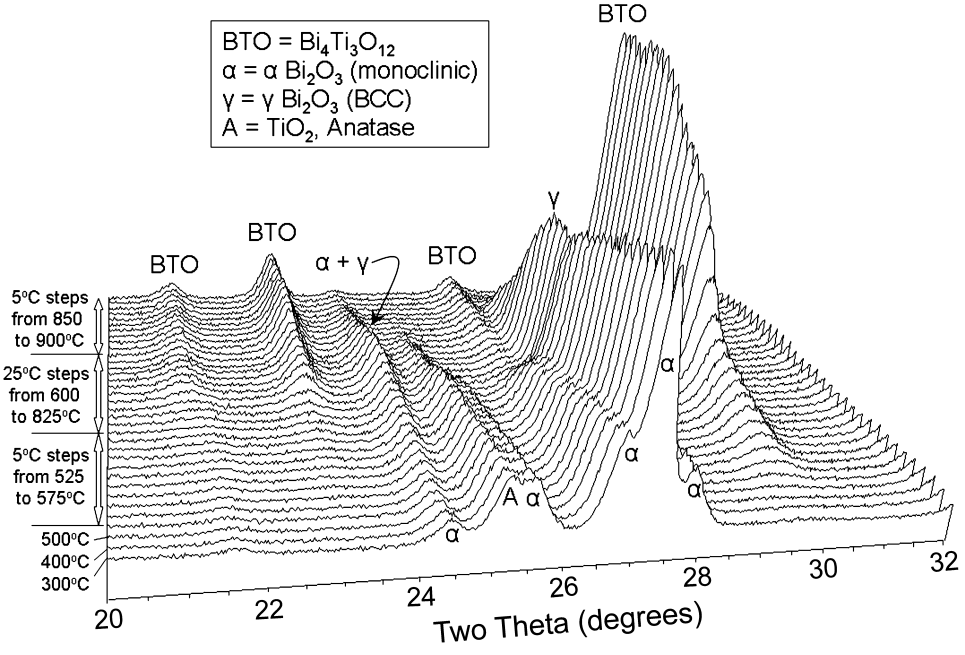

Fig. 10 In-situ XRD measurement of the reaction mechanisms that produce $Bi_4Ti_3O_{12}$ from mixed oxide powders

the tetragonal polymorph, and therefore suggest that other layered structures are potentially technologically important oxide ion conductors.

The Aurivillius ceramics, also 2-dimensional in nature, are composed of perovskite-like layers sandwiched between $[Bi_2O_2]^{2+}$ sheets and include variants that incorporate 1, 2, 3, and up to 8 perovskite octahedral layers. The BIMEVOX fast ion conductors represent the 1-layer variant and have been well characterized [31]. Early reports indicated that the 3- and 4-layer variants were also technologically important fast ion conductors [34–38]. In addition, the non-centrosymmetric 2-, 3-, etc. layer Aurivillius variants have been under intense study for several years for application in ferroelectric memory devices, primarily as a result of their exceedingly low ferroelectric fatigue.

Possible applications of the Aurivillius ceramics in electrochemical devices and RAM modules sparked several studies of the kinetics of formation of several of the Aurivillius phases in bulk and film forms. The formation of $Bi_4Ti_3O_{12}$ has been studied by several authors using differential thermal analysis (DTA) and ambient XRD [39–42]. The reaction as followed using in-situ XRD is shown in Fig. 10, which shows Bi_2O_3 reacting with anatase to form directly the Aurivillius phase $Bi_4Ti_3O_{12}$ with no intermediates [43]. An interesting feature in the in-situ XRD data is the transformation of α Bi_2O_3 (monoclinic) to the γ (BCC) polymorph at ~680°C. While this reaction has never been observed on heating, the $\delta \rightarrow \gamma \rightarrow \alpha$ sequence has been clearly established on cooling [44–46]. The fluorite high temperature δ phase of Bi_2O_3 can be stabilized by a wide range of cation additions [44] and therefore the data in Fig. 10 indicate that small concentrations of Ti in solution with Bi_2O_3 stabilize the γ polymorph.

The reaction kinetics for $Bi_4Ti_3O_{12}$ growth were determined using isothermal in-situ XRD measurements by rapidly heating the specimen to a target temperature, then collecting XRD patterns as a function of time at constant temperature. Full Rietveld analysis of the data was performed to determine the quantity of each phase present as a function of time. The "standardless quantitative analysis" using the Rietveld whole-pattern fitting approach has been well established [47, 48] and was executed using the commercial code TOPAS from Bruker AXS [49]. Figure 11 shows the results from the isothermal experiments. The concentration of $Bi_4Ti_3O_{12}$is shown as a function of time at each temperature, to which an appropriate model can be fitted to extract the rate constant at each temperature, and then the Arrhenius behavior was used to determine the activation enthalpy. The in-situ XRD measurements yield an activation enthalpy of 243 kJ/mol, in good agreement with the results of Jung et al. (263 kJ/mol) [39] who also used XRD but quenched their specimens and performed room temperature XRD.

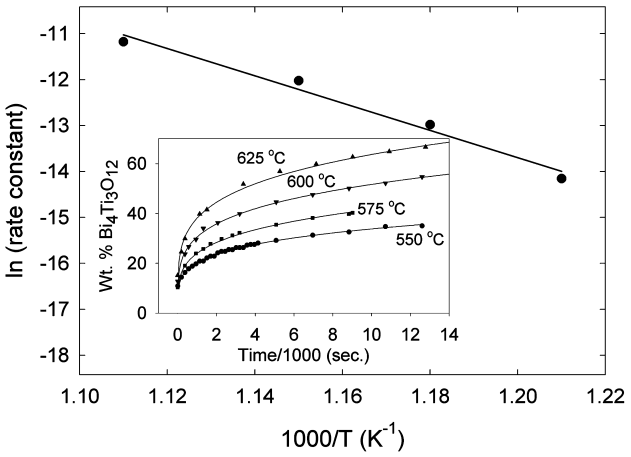

Fig. 11 Arrhenius plot of the rate constants for the reaction to form $Bi_4Ti_3O_{12}$ determined using isothermal in-situ XRD measurements. Inset shows the formation of $Bi_4Ti_3O_{12}$ as a function of time at four temperatures determined using standardless quantification by Rietveld analysis

Additional work on the Aurivillius phases included attempts to understand the reported disordering transformation that results in fast ion conduction for '$Bi_2Sr_2Nb_2$(Ga or Al)O_{12-x},' [34–36, 38, 50] a problem well-suited for in-situ studies. $Bi_2Sr_2Nb_2TiO_{12}$ is a centrosymmetric Aurivillius phase that crystallizes in space group 14/mmm and has been carefully characterized using both X-ray and neutron powder diffraction [51–54]. Thomas et al. [38] and Kendall et al [34–36, 50] suggested that full replacement of Ti by Ga or Al creates oxygen vacancies that fully disorder at approximately 775°C.

The measured total conductivity for specimens of composition $Bi_2Sr_2Nb_2$(Ga or Al)O_{12-x} is shown in the inset in Fig. 12, which, at first glance, is similar to the behavior of other conductors that undergo order-disorder transformations. Snedden, et al [54] first showed that the XRD data from specimens with full replacement of Ti by Ga could not be modeled using the 14/mmm space group and that the specimens contained the β polymorph of Bi_2O_3. Again in-situ XRD (as well as microscopy, DSC, microprobe, etc.) was used to develop a more clear understanding of the system [55].

Figure 9 shows the in-situ diffraction results for '$Bi_2Sr_2Nb_2AlO_{12-x}$' that was sintered in a powder bed for 48 hours at 1025°C. The XRD data show that the specimen contains the β and γ polymorphs of Bi_2O_3 at room temperature to ~675°C, followed by full transformation to the γ form. As the temperature is increased, the expected transformation to the high conductivity δ polymorph begins at 725°C and goes to completion at 780°C, in excellent agreement with the conductivity data measured on heating.

NiO is an important material for solid oxide and molten carbonate fuel cells as well as many catalyst applications. In

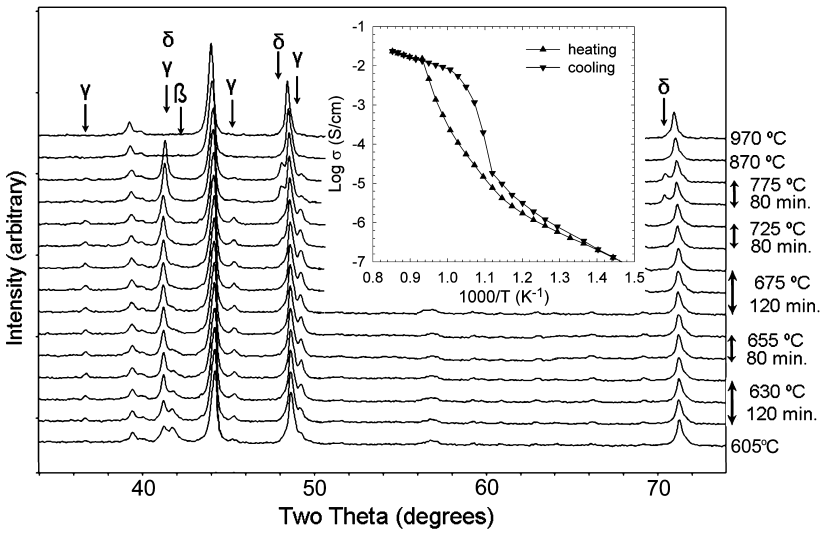

Fig. 12 In-situ XRD measurement of the two-phase mixture obtained by equilibrating '$Bi_2Sr_2Nb_2AlO_{12-x}$.' The phase transformations in the Bi_2O_3 minor phase are reflected in the measured conductivity of the specimen (inset)

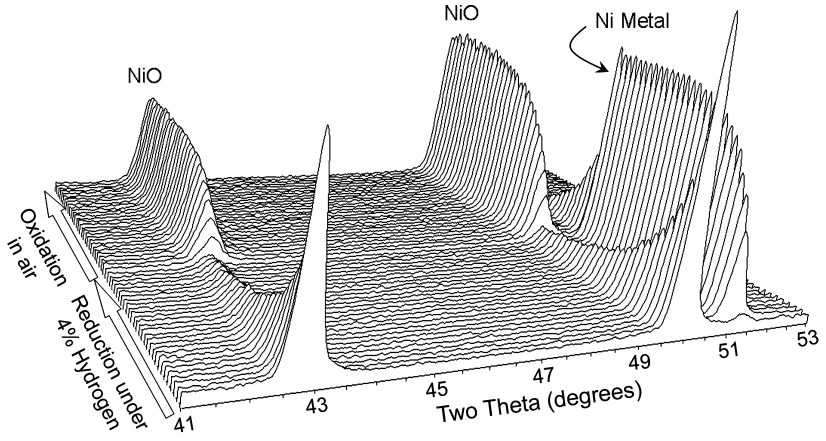

Fig. 13 Reduction and reoxidation of a NiO/YSZ fuel cell anode composite measured using in-situ XRD

the case of solid oxide fuel cells, porous composite NiO/YSZ anodes are of interest, and both nano and micro-crystalline NiO are important in catalyst applications. Several in-situ diffraction studies have been undertaken to track the conversion of NiO to Ni using X-rays [56, 57] and neutrons [58].

In the case of NiO/YSZ fuel cell anodes, independent studies of the reduction and reoxidation behavior were performed using in-situ XRD [56] and differential thermal analysis [59]. Figures 13 and 14 show the in-situ XRD result, where Rietveld analysis was used to quantify the phases present as a function of time and atmosphere during isothermal measurements. Reduction of the NiO was accomplished using dry 4% H_2 in He, and reoxidation was monitored after flooding the in-situ XRD furnace with dry air. The in-situ XRD result is in excellent agreement with the thermal analysis work of Waldbillig et al. [59]. Both experimental approaches yielded activation energies for reoxidation that were ∼10 kJ/mol higher than for reduction.

Another example of in-situ XRD studies under carefully controlled atmosphere is shown in Fig. 15. During investigations of hydrogen cycling in TiZrNi quasicrystalline alloys [60, 61] under inert gas, the experiments required installing an oxygen gettering element in the X-ray furnace adjacent

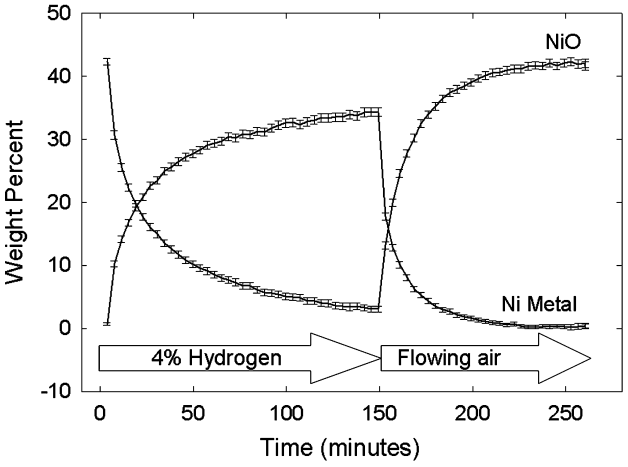

Fig. 14 Quantification of the data shown in Fig. 11 using standardless Rietveld analysis. Error bars shown are ±1 estimated standard deviation from the refinements

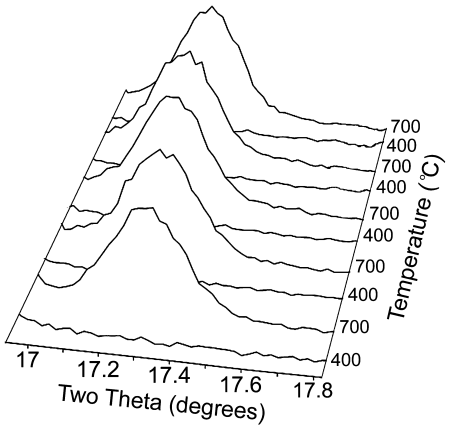

Fig. 15 In-situ XRD data for the reversible $\alpha \leftrightarrow \beta$ phase transition in Ti metal over the course of 10 cycles between 400 and 700°C

to the specimen. Figure 15 shows the XRD data for the reversible $\alpha \leftrightarrow \beta$ phase transition in Ti over the course of 10 cycles between 400 and 700°C, and demonstrated that exceedingly low PO_2 could be maintained throughout the duration of the experiment when using an inert blanket gas.

High temperature diffraction is of course well-suited for structure solution and refinement of high temperature polymorphs, in particular those that can not be effectively quenched to room temperature. An example is shown in Fig. 16 for $In_2(WO_4)_3$, which might find application in electrical and optical devices [62]. The $In_2(WO_4)_3$ phase undergoes a monoclinic to orthorhombic phase transition at ~250°C. The structures of the low and high temperature polymorphs were solved using the in-situ data, and the final Rietveld refinements and structures are shown in Fig. 16.

Among the most recent structure type considered for oxide ion conduction is the apatite structure that is written $A_{10-x}(MO_4)_6O_{2\pm\delta}$ with A=Si or Ge and M = rare earth or alkaline earth cations. Two very recent reviews by Kharton et al. [31] and Higuchi et al. [63] describe the structures and conductivity. A final example of the in-situ XRD method is the measurement of the thermal expansion of $Dy_{4.67}Si_3O_{13}$

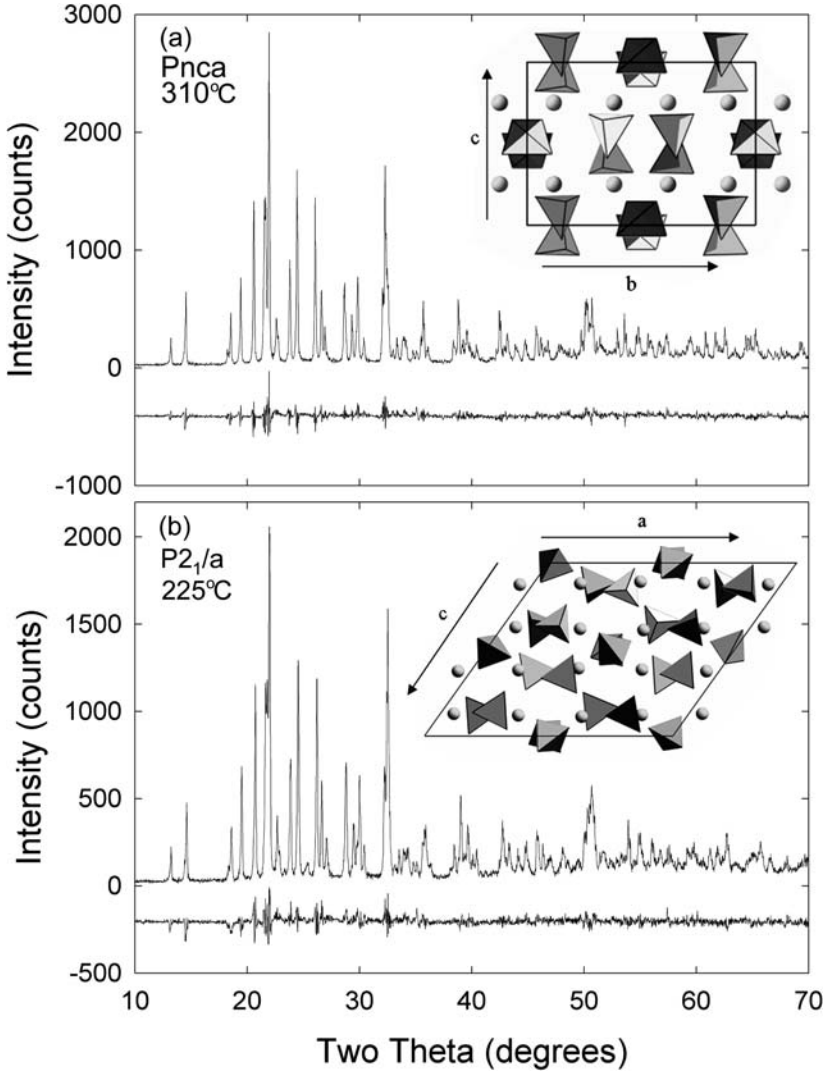

Fig. 16 High temperature structures of $In_2(WO_4)_3$ determined using in-situ XRD and Rietveld analysis. Observed and difference patterns are shown for both structures, as well as structure schematics

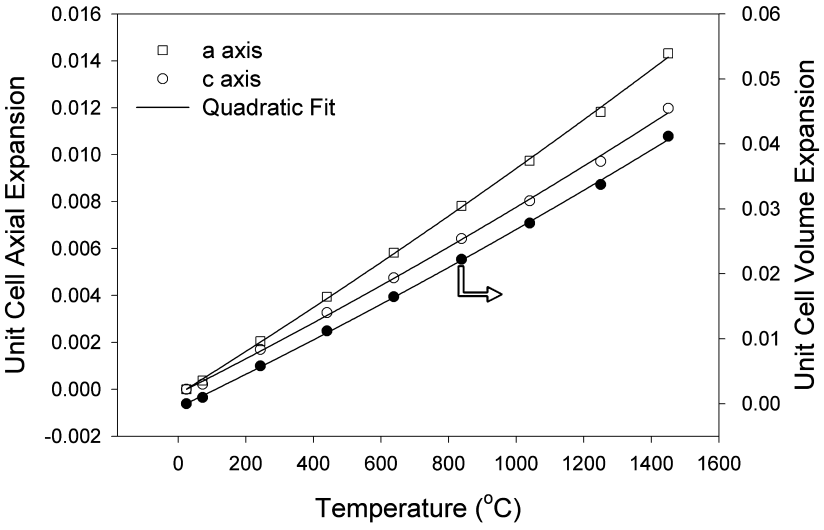

Fig. 17 Thermal expansion of the rare earth apatite $Dy_{4.67}Si_3O_{13}$ out to 1450°C. Both axial and volume expansion are shown

to 1450°C shown in Fig. 17 [64]. The simplicity in measuring the anisotropy in thermal expansion using powders, instead of single crystals, has prompted measurements of field-induced strain in electroactive materials including lead zirconate titanate (PZT) [11] and modified lead magnesium niobate (PMN) [65].

Elegant experiments by Zorn et al. [11] used a position-sensitive detector to capture the cyclic strain in PZT as a function of time under a 50 Hz drive field. The measurement was performed by storing the XRD data in 16 bins that each represent a time slice of the ac field. The resulting data shows that the XRD peaks shift as a result of the field-induced strain in the crystallites, and the authors were able to determine the effective single-crystal electrostrictive coefficients. A similar study was performed on PMN electrostrictors, but using neutron diffraction under static fields and controlled temperature and prestress [65]. Again, measuring the field response of several different diffraction peaks allowed a full determination of the effective single-crystal electrostrictive coefficients. Both studies provide the response of the grains in the polycrystalline bodies, and therefore an estimate of the reduction in total strain resulting from the grain boundary regions, thus guiding the ceramic processing methodology to optimize the performance.

Complementary techniques and future opportunities

High temperature optical microscopy, TEM, and environmental SEM (among others) allow direct observation of sintering, wetting angles, dislocation motion, phase development, crystal growth, orientation relationships, and even electrical, mechanical, and field emission behavior [66–69]. Of course, complementing these techniques with in-situ XRD, and vice-versa, can be quite valuable in many cases. The environmental SEM is quite likely to find widespread use as a high temperature in-situ analysis tool, especially when equipped with a turn-key electron backscattered diffraction system which can be used for both phase identification and grain orientation mapping.

In-situ thin film characterization, in particular high resolution diffraction and X-ray reflectivity, is quite uncommon and restricted to synchrotron and neutron sources. Complete experimental facilities for temperature and atmosphere controlled high resolution diffraction are available (for example [70]) at some of the synchrotron and neutron sources. In addition, several examples of in-situ X-ray reflectivity have been published, including the electric field response of polycrystalline PZT thin films for random access memory [71]. Recent extraordinary advances in low-power high-brilliance laboratory X-ray sources [72] and crystal optics [73] have enhanced laboratory facilities for thin film characterization, and will likely facilitate in-situ thin film analysis in the near future.

The current state of the lateral resolution for X-ray analysis is some tens of microns in the laboratory to some tens of nanometers at the synchrotron. Although temperature-controlled microdiffraction experiments are not common, Hackemann and Pfeiffer have demonstrated that combining microdiffraction optics with a 2-D detector and load frame provided in-situ data as a function of mechanical loading for PZT [74]. Their measurements were in fact sufficient to quantify the effects of domain switching in the vicinity of cracks in soft PZT using a standard laboratory X-ray source.

Summary

Recent vast improvements in laboratory X-ray instrumentation have made atmosphere-controlled high temperature studies accessible to the casual user interested in bulk

behavior or polycrystalline films. In-situ analysis is ideally suited for the study of systems that can not be reliably quenched to room temperature, but can also be used as a highly efficient means of mapping the structure—processing—performance links in materials systems. The ability to study the dynamics of a material response, including cyclic responses, has been demonstrated for a range of variables including temperature, oxygen partial pressure, mechanical load, and electric field.

The use of synchrotron and neutron sources for in-situ studies provides the ultimate extension of time, size, and lateral resolution for diffraction experiments, as well as an array of related scattering and spectroscopy methods. The continued evolution of the in-situ diffraction and scattering methods at both the national facilities and in the laboratory will likely make the techniques commonplace, extending our depth of understanding of complex materials systems.

Acknowledgments The National Science Foundation supported the instrument development and studies of Aurivillius ceramics under Contract # DMR-9983801. The barium indate in-situ neutron studies were conducted at the GPPD beamline at the Intense Pulsed Neutron Source, Argonne National Lab, supported by the U.S. Department of Energy, BES-Materials Sciences, under contract W-31-109-Eng-38.

References

1. R.J. Angel, R.T. Downs, and L.W. Finger, High temperature High pressure diffractometry, in P.H. Ribbe (ed.) *High Temperature and High Pressure crystal chemistry*, vol 41, Mineralogical Society of America, Washington, DC, (2000), p. 559–594.
2. R.B.V. Drele, Neutron powder diffraction, in P.H. Ribbe (ed.) *Modern Powder Diffraction*, vol 20, The Mineralogical Society of America, Washington, DC, (1989), p. 333–367.
3. Y. Fei and Y. Wang, High pressure and high temperature powder diffraction, in P. H. Ribbe (ed.) High Temperature and High Pressure Crystal Chemistry, vol 41, Mineralogical Society of America, Washington, DC, (2000), p. 521–551.
4. R.C. Peterson and H. Yang, High temperature devices and environmental cells for X-ray and neutron diffraction experiments, in P. H. Ribbe (Ed.) *High temperature and high pressure crystal chemistry*, vol 41, Mineralogical Society of America, Washington, DC, (2000) p. 425–442.
5. D.D.L. Chung, P.W. DeHaven, H. Arnold, and D. Gosh, *X-ray Diffraction at Elevated Temperatures*, VCH Publishers, New York, p. 268 (1993).
6. M. Dapiaggi, G. Artioli, and L. Petras, *Journal Rigaku*, **19**, 35–41 (2002).
7. M.D. Dolan, S. Zdzieszynski, and S.T. Misture, *Advances in X-ray Analysis*, **46**, 50 (2002).
8. L. Margulies, M.J. Kramer, R.W. McCallum, S. Kycia, D.R. Haeffner, J.C. Lang, and A.I. Goldman, *Review of Scientific Instruments*, **70**, 3554–3562 (1999).
9. S.T. Misture, *Measurement Science and Technology*, **14**, 1091–1098 (2003).
10. T. Blanton, M. Lelental, S. Zdzieszynski, and S. Misture, *Advances in X-Ray Analysis*, **45**, 371–376 (2002).
11. G. Zorn, *Ferroelectrics* **55**, 759–762 (1984).
12. H.P. Klug and L.E. Alexander, *X-ray Diffraction Procedures*, John Wiley & Sons, New York, (1974) p. 966.
13. M.D. Dolan, S. Zdzieszynski, and S.T. Misture, *Advances in X-Ray Analysis*, **46** 50–55 (2003).
14. S.T. Misture, *Advances in X-Ray Analysis*, **45**, 166–171 (2002).
15. S.T. Misture and M. Haller, *Advances in X-Ray Analysis*, **43**, 279–284, (2000).
16. T. Mitsunaga, M. Saigo, and G. Fujinawa, *Powder Diffraction*, **17**, 173–177, (2002).
17. R.D. Deslattes, J.L. Staudenmann, L.T. Hudson, A. Henins, and J.P. Cline, *Advances in X-Ray Analysis*, **40**, 221–231 (1998).
18. X. Chen, J. Yu, and S.B. Adler, *Chem. Mater.*, in press (2005).
19. N. Grunbaum, L. Mogni, F. Prado, and A. Caneiro, *J. Solid State Chem.*, **177**, 2350–2357 (2004).
20. S. Miyoshi, A. Kaimai, H. Matsumoto, K. Yashiro, Y. Nigara, T. Kawada, and J. Mizusaki, *Solid State Ionics*, **175**, 383–386 (2004).
21. F. Prado, N. Grunbaum, A. Caneiro, and A. Manthiram, *Solid State Ionics*, **167**, 147–154 (2004).
22. S. Uhlenbruck and F. Tietz, *Mat. Sci. Eng.*, B **107**, 277–282 (2004).
23. S.B. Adler, *J. Amer. Ceram. Soc.*, **84**, 2117–2119 (2001).
24. S. Miyoshi, J.-O. Hong, K. Yashiro, A. Kaimai, Y. Nigara, K. Kawamura, T. Kawada, and J. Mizusaki, *Solid State Ionics*, **161**, 209 (2003).
25. A. Fossdal, M. Menon, I. Waernhus, K. Wiik, M.-A. Einarsrud, and T. Grande, *J. Amer. Ceram. Soc.*, **87**, 1952–1958 (2004).
26. R. Caciuffo, D. Rinaldi, G. Barucca, J. Mira, J. Rivas, M.A. SenarisRodriguez, P.G. Radaelli, D. Fiorani, and J.B. Goodenough, *Phys. Rev. B*, **59**, 1068–1078 (1999).
27. E. Bucher, W. Sitte, I. Rom, I. Papst, W. Gorgger, and F. Hofer, *Solid State Ionics*, **152–153**, 417–421 (2002).
28. J.B. Goodenough, J.E. Ruiz-Diaz, and Y.S. Zhen, *Solid State Ionics*, **44**, 21–31 (1990).
29. S.B. Adler, J.A. Reimer, J. Baltisberger, and U. Werner, *Journal of the American Ceramic Society*, **116**, 675–681 (1994).
30. V.V. Kharton, I.P. Marozau, N.P. Vyshatko, A.L. Shaula, A.P. Viskup, E.N. Naumovich, and F.M.B. Marques, Materials Research Bulletin, **38**, 773 (2003).
31. V.V. Kharton, F. M. B. Marques, and A. Atkinson, *Solid State Ionics*, **174**, 135 (2004).
32. S.A. Speakman, J.W. Richardson, B.J. Mitchell, and S.T. Misture, *Solid State Ionics*, **149**, 247–259 (2002).
33. H. Yamamura, Y. Yamada, T. Mori, and T. Atake, *Solid State Ionics*, **108**, 377–381 (1998).
34. K.R. Kendall, C. Navas, J.K. Thomas, and H.-C. zur Loye, *Solid State Ionics*, **82**, 215–223 (1995).
35. K.R. Kendall, C. Navas, J.K. Thomas, and H.-C. zur Loye, *Chemistry of Materials*, **8**, 642–649 (1996).
36. K.R. Kendall, J.K. Thomas, and H.C.zur Loye, *Solid State Ionics*, **70/71**, 221–224 (1994).
37. J.K. Thomas, M.E. Anderson, W.E. Krause, and H.C.zur Loye, Oxygen ion conductivity in a new class of layered bismuth oxide compounds, in G.-A. Nazri, J.-M. Tarascon, M. Schreiber (Eds.), Solid State Ionics III, *Proceedings of the Materials Research Society Society Fall Meeting*, vol 293, Materials Research Society, Boston, MA, (1993), pp. 295–299.
38. J.K. Thomas, K.R. Kendall, and H.-C. zur Loye, *Solid State Ionics*, **70–71**, 225 (1994).
39. S.-Y. Jung, S.-J. Hwang, and Y.-M. Sung, *Journal of Crystal Growth*, **254**, 92 (2003).
40. W.-C. Kwak and Y.-M. Sung, *J. Mater. Res.*, **17**, 1463–1468 (2002).
41. W.-C. Kwak and Y.-M. Sung, *Journal of the European Ceramic Society*, **24**, 1603 (2004).
42. C.-H. Lu and J.-T. Lee, *Ceram. Int.*, **24**, 285–291 (1998).
43. M.S. Peterson, C.A. Say, S.A. Speakman, and S.T. Misture, *Advances in X-Ray Analysis*, **46**, 226–231 (2003).

44. N.M. Sammes, G.A. Tompsett, H. Nafe, and F. Aldinger, *Journal of the European Ceramic Society*, **19**, 1801–1826 (1999).
45. P. Shuk, H.-D. Wiemhofer, U. Guth, W. Gopel, and M. Greenblatt, *Solid State Ionics*, **89**, 179–196 (1996).
46. T. Takahashi and H. Iwahara, *Materials Research Bulletin*, **13**, 1447–1453 (1978).
47. R.J. Hill, *Applied Crystallography*, **17**, 65–86 (1998).
48. H. Toraya, *Journal of Applied Crystallography*, **33**, 1324–1328 (2000).
49. Diffrac Plus: TOPAS: General Profile Structure and Analysis Software for Powder Diffraction Data, in Bruker AXS, Karlsruhe, Germany, 2000.
50. K.R. Kendall, J.K. Thomas, and H.C.zur Loye, *Chemistry of Materials*, **7**, 50–57 (1995).
51. M.S. Haluska and S.T. Misture, Cation site mixing for strain relief in Three-Layer aurivillius ceramics, in M. Greenblatt, M. A. Alario-Franco, M. S. Whittingham, G. Rohrer (Eds.), *Materials Research Society Fall Meeting,* vol 755, Materials Research Society, Boston, MA, pp. 103–108 (2003).
52. M.S. Haluska and S.T. Misture, *Journal of Solid State Chemistry*, **177**, 1965–1975 (2004).
53. C.H. Hervoches and P. Lightfoot, *Journal of Solid State Chemistry*, **153**, 66 (2000).
54. A. Snedden, S. M. Blake, and P. Lightfoot, *Solid State Ionics*, **156**, 439 (2003).
55. S.A. Speakman, M.S. Haluska, C.A. Say, and S.T. Misture, *Solid State Ionics* (in press) (2005).
56. M.D. Dolan and S.T. Misture, *Rigaku Journal*, **21**, 12–16 (2004).
57. J.T. Richardson, R.M. Scates, and M.V. Twigg, *Applied Catalysis A: General*, **267**, 35 (2004).
58. S. Vogel, E. Ustundag, J.C. Hanan, V.W. Yuan, and M.A.M. Bourke, *Materials Science and Engineering A: Structural Materials: Properties, Microstructure and Processing* **333**, 1 (2002).
59. D. Waldbillig, A. Wood, and D.G. Ivey, *Solid State Ionics*, **176**, 847 (2005).
60. R.M. Stroud, K.F. Kelton, and S.T. Misture, *Journal of Materials Research*, **12**, 434–438 (1997).
61. R.M. Stroud, A.M. Viano, P.C. Gibbons, K.F. Kelton, and S.T. Misture, *Applied Physics Letters*, **69**, 2998 (1996).
62. A.P. Richard and D.D. Edwards, *Journal of Solid State Chemistry*, **177**, 2740 (2004).
63. M. Higuchi, Y. Masubuchi, S. Nakayama, S. Kikkawa, and K. Kodaira, *Solid State Ionics*, **174**, 73 (2004).
64. S.T. Misture, S.P. Harvey, R.T. Francy, Y. Gao, S. DeCarr, and S.C. Bancheri, *Journal of Materials Research*, 2330–2335 (2004).
65. S.T. Misture, S.M. Pilgrim, J.C. Hicks, C.T. Blue, E.A. Payzant, and C.R. Hubbard, *Applied Physics Letters*, **72**, 1048 (1998).
66. L M. Hsiung, A.J. Schwartz, and T.G. Nieh, *Intermetallics* **12**, 727–732 (2004).
67. H. Marzagui and T. Cutard, *Journal of Materials Processing Technology*, **155–156**, 1474 (2004).
68. S.C. Wang and Y. Li, *Journal of Magnetism and Magnetic Materials*, **285**, 177–182 (2005).
69. Z.L. Wang, P. Poncharalb, and W.A.d. Heerb, *Journal of Physics and Chemistry of Solids*, **61**, 1025–1030 (2000).
70. H. Tajiri, K. Sumitani, S. Nakatani, T. Takahashi, K. Akimoto, H. Sugiyama, X. Zhang, and H. Kawata, *Applied Surface Science*, **237**, 641 (2004).
71. J.-L. Cao, A. Solbach, and U. Klemradt, *Physica* B, in press (2005).
72. C. Jensen, S.M. Elliott, S.D. Liddiard, A. Reyes-Mena, M. Moras, and D.C. Turner, *Advances in X-ray Analysis*, **47**, 64–69 (2004).
73. D.K. Bowen and B.K. Tanner, *High Resolution X-ray Diffractometry and Topography*, Taylor & Francis, London, (1998), p. 252.
74. S. Hackemann, W. Pfeiffer, and J. European *Ceramic Soc.*, **23**, 141–151 (2003).